Impact of maltene and asphaltene fraction on mechanical behavior and microstructure of bitumen

B. Hofko, L. Eberhardsteiner, J. Füssl, H. Grothe, F. Handle, M. Hospodka, D. Grossegger, S. N. Nahar, A. J. M. Schmets & A. Scarpas

Materials and Structures

ISSN 1359-5997
Volume 49
Number 3

Mater Struct (2016) 49:829-841
DOI 10.1617/s11527-015-0541-6

Springer

Materials and Structures (2016) 49:829–841
DOI 10.1617/s11527-015-0541-6

ORIGINAL ARTICLE

Impact of maltene and asphaltene fraction on mechanical behavior and microstructure of bitumen

B. Hofko · L. Eberhardsteiner · J. Füssl · H. Grothe · F. Handle · M. Hospodka · D. Grossegger · S. N. Nahar · A. J. M. Schmets · A. Scarpas

Received: 13 June 2014 / Accepted: 20 January 2015 / Published online: 31 January 2015

Abstract As a widely accepted concept, bitumen consists of four fractions that can be distinguished by their polarity. Highly polar asphaltene micelles are dispersed in a viscous phase of saturates, aromatics and resins (maltene phase). Different concentrations of asphaltenes in the bitumen result in a range of mechanical response properties. In an interdisciplinary study the impact of the maltene phase and asphaltenes on the linear viscoelastic behavior and the microstructure of bitumen were analyzed by creep recovery testing in a DSR and by atomic force microscopy (AFM). Therefore, bitumen was separated into the maltene and asphaltene fractions and artificial bitumen samples with different, pre-defined asphaltene concentrations were produced and investigated. It was found that the artificially produced, precipitated bitumen samples can be regarded as a representative, bitumen-like material in terms of mechanical behavior and microstructure. Asphaltenes play an important role in the typical viscoelastic behavior of bitumen being mainly responsible for stiffness and elasticity. Also, their concentration appears to be correlated to the occurrence and shape of the bee-like inclusions which can be typically observed by AFM.

Keywords Bitumen composition · DSR · AFM · Maltene · Asphaltene · Microstructure

B. Hofko (✉) · L. Eberhardsteiner · J. Füssl · H. Grothe · F. Handle · M. Hospodka · D. Grossegger
Vienna University of Technology, Karlsplatz 13, 1040 Vienna, Austria
e-mail: bernhard.hofko@tuwien.ac.at
URL: http://www.ivws.tuwien.ac.at

S. N. Nahar · A. J. M. Schmets · A. Scarpas
Section of Road and Railway Engineering, Faculty of Civil Engineering & Geosciences, Delft University of Technology, Stevinweg 1, 2628 CN Delft, The Netherlands

1 Introduction and motivation

Over the course of the twentieth century, modern road building techniques emerged from tar-bound macadam construction, abolishing tar in favor of bitumen for health and ecological reasons in the fall of the century. Today, bitumen is the most important binder material in road engineering in Europe.

The economic crisis in 2009 imposed dramatically increased demands on engineering, as the available budgets for transportation were cut from around 1 % of the GDP to around 0.85 %. Additionally, the modal split of this budget for road building and maintenance was reduced from around 70–60 % [1]. Economic and ecologic considerations point to one demand: sustainability. Thus, resource efficiency and recycling are topics of ongoing research.

However, both long-term performance and asphalt concrete recycling are strongly linked to the understanding of the bitumen microstructure and ageing of

bitumen. On one hand, it is naturally important to understand microstructure to create high performance and durable products, and on the other hand, countering the effects of ageing is necessary for efficient recycling.

European standards define bitumen as a "*virtually involatile, adhesive and waterproofing material derived from crude petroleum or present in natural asphalt, which is completely or nearly completely soluble in toluene, and very viscous or nearly solid at room temperature*" [2]. The chemical perspective describes bitumen as a composite material that can easily be separated into two major fractions by solvent extraction with *n*-heptane: (a) the insoluble fraction or asphaltenes, and (b) the soluble fraction, the maltenes [3]. The soluble fraction can be split into three phases by column chromatography: saturates, aromatics (also apolar aromatics), and resins (also polar aromatics) [4–6]. The separation is based on similar chemical properties regarding polarity, but size and aromaticity of the molecules also contribute.

Regarding the bitumen microstructure, one of the two widely accepted concept states that the asphaltenes aggregate and are stabilized by smaller, less polar molecule as micelles in a matrix of maltenes [5, 7–10]. The existence of ordered agglomerates has been proven by small angle X-ray scattering and small angle neutron scattering experiments [11–13] and the nature of asphaltene agglomeration is well established for different solvents, leading to problems and discussions regarding the size of the asphaltenes and their agglomerates [11, 14–16]. The existence of a bitumen microstructure and its visualization was performed by various techniques, ranging from confocal laser scanning microscopy (CLSM) and scanning electron microscopy (SEM) to atomic force microscopy (AFM) [17–26]. A detailed comparison of various imaging technique was performed by Bearsley et al. [18]. It is important to note that the particles found by CLSM and AFM are of the same size range between 1 and 10 µm in general.

The second model explains the expression of micro-structural features in the µm range as the crystallization of waxes on the bitumen surface. This argumentation is based on several studies, proposing a strong correlation between wax/saturates content and the frequency of occurrence of structural features [5, 22, 27, 28]. Additionally, mixed models have developed by combining both asphaltene precipitation and wax crystallization approaches [29].

The understanding of the influence of bitumen on the material properties of asphalt mixes can be assessed through multi-scale modeling. When applying multi-scale models to asphalt mixes, bitumen has been seen as the lowest level of observation [30–34] so far, and thus, bitumen considered a homogeneous material in terms of structure and mechanical behavior (see Fig. 1).

In recent studies [35, 36], the multi-scale model has been extended to take into account the microstructure of bitumen and its influence on the mechanical behavior from binder up to the macroscale level. To obtain information on the mechanical behavior of the bitumen constituents, bitumen samples were separated into *n*-heptane solubles (maltene phase) and insolubles (asphaltenes) and artificial bitumen with pre-defined asphaltene concentrations from 0 to 30 wt% asphaltenes were produced from the constituents. These artificial bitumen samples were produced by precipitating maltenes and asphaltenes which are dissolved in toluene (see Sect. 3.2 for details). The artificial bitumen samples were tested mechanically in creep-recovery (CR) tests at different temperatures to directly determine the viscoelastic behavior of the maltene phase and indirectly of the asphaltenes. Since this approach, to create artificial bitumen from maltenes and asphaltenes has not been used for mechanical characterization of the material yet, the study presented in this paper shows an in-depth analysis of mechanical behavior and microstructure of the original bitumen and the artificially produced, precipitate bitumen samples.

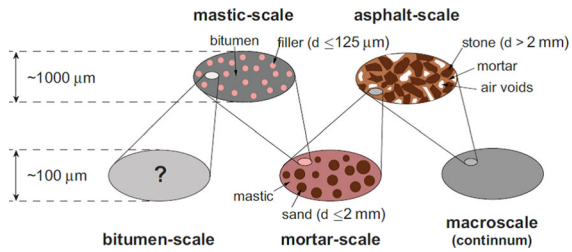

Fig. 1 Multi-scale model of hot mix asphalt according to [30–34]—microstructure of bitumen not yet considered

2 Objectives and approach

The main objective of the presented research is to investigate whether the process of separating bitumen by *n*-heptane extraction and producing artificial bitumen samples from their constituents leads to valid bitumen-like materials in terms of the microstructure and linear viscoelastic (LVE) behavior. In addition, the impact of the asphaltene concentration on the microstructure and LVE behavior will be analyzed.

The following approach is taken:

- Separate bitumen samples by *n*-heptane extraction based on ASTM Standard 4124 [4].
- Produce artificial bitumen samples from the *n*-heptane constituents (maltene phase and asphaltenes) with different pre-defined asphaltene concentrations.
- Carry out static creep-recovery (CR) tests on a dynamic shear rheometer to gather information on the LVE behavior of the original bitumen and artificial bitumen samples.
- Investigate the samples in the AFM following a standardized procedure to obtain the microstructure of the samples.

3 Materials and test program

3.1 Bitumen

For the experiment, an unmodified, straight-run bitumen 70/100 pen (B287A) was used. The asphaltene concentration of the original bitumen was found to be 8.73 wt%. All tests for determination of the parameters presented in Table 1 were performed in accordance to the current European Standards [37–40].

Table 1 Main characteristics of the bitumen

Parameter	B287A
Penetration (1/10 mm)	91
Softening point ring & ball (°C)	46.6
SHRP PG (°C)	58–22

3.2 Bitumen separation and artificial bitumen samples

Bitumen can be separated into two major fractions: (a) the *n*-heptane soluble phase, which is generally called maltene phase, appearing as a viscous liquid at room temperature, and (b) the *n*-heptane insoluble phase, called asphaltene phase, which exhibits solid or almost solid properties. The bitumen samples used in this study were prepared and analyzed gravimetrically by an experimental procedure based on the bitumen separation by *n*-heptane extraction as proposed by ASTM 4124 [4]. Hereby, around 10 g of bitumen are weighed into a 2 l Erlenmeyer flask and around 300 ml of *n*-heptane were added. Through stirring, a good dispersion of the bitumen was assured. The flask was then heated to 90 °C and kept at that temperature for around 1.5 h. Afterwards, the bottle was set aside and left for cooling and sedimentation of particles overnight. The next day, the dispersion was filtered through a Büchner-funnel and the filter paper was folded and inserted into a Soxhlet extractor filled with around 700 ml of *n*-heptane. The extraction was kept running for 72 h. Afterwards, the liquid phase was combined with the filtrate. The solvent was removed by evaporation (160 °C, 10 mbar, 50 min) and the maltenes were weighed and taken up in 200 ml of toluene, thus we obtained a toluene solution of maltenes with known concentration values. The extractor was filled with toluene and the extraction process started again to obtain the asphaltene phase after another 72 h. The solvent was removed by evaporation (110 °C, 10 mbar, 50 min) and the solid residue was weighed and taken up in 50 ml of toluene. Then the solutions were mixed to create artificial bitumen with a defined asphaltene concentration after evaporation of the toluene.

3.3 Mechanical testing by DSR

To determine mechanical creep properties of the original and artificial bitumen samples the dynamic shear rheometer (DSR, see Fig. 2) was chosen as experimental setup for static creep shear tests—so called CR tests. While a constant torque M is applied statically for 1,800 s on a bitumen film (diameter $d = 25$ mm, height $h = 1$ mm), the deflection $\gamma(t)$ is measured. From $\tau = 2M/\pi r^3$, with $r = d/2$, and the strain

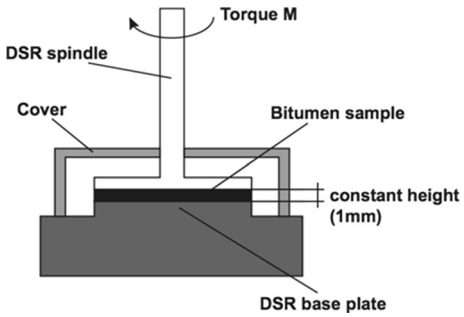

Fig. 2 Creep-recovery test using DSR experimental equipment

$$\gamma(t) = \frac{r}{\pi}\varphi(t) \tag{1}$$

the creep compliance

$$J_{\exp}(t) = \frac{\gamma(t)}{\tau} \tag{2}$$

can be obtained. These tests were performed at predefined temperatures in the range of −5 to +15 °C. In Table 2, the experimental program is provided.

3.4 Atomic force microscopy (AFM)

3.4.1 Sample preparation, measuring conditions and instrumental settings

The bitumen specimens for the AFM were prepared by applying 20 ± 3 mg of sample material using a spatula on 12 mm steel substrates (0.4 ± 0.08 mm thickness) and then they were heated for 30 s at 100 °C on a heater plate. The temperature was altered to 200 °C for the bitumen samples containing 30 % asphaltene and prepared by following the same procedure. The temperature and the heating time was sufficient to melt the bitumen to provide a smooth film. Then the specimens were thermally conditioned inside a preheated oven at 100 °C for 60 min. Prior to AFM imaging, the specimens were allowed to equilibrate at the imaging temperature (25 °C) for 24 h.

Table 2 Experimental program for CR tests on original and artificial bitumen samples

Asphaltene content	Test temperature		
	−5 °C	+5 °C	+15 °C
0 wt%	•	•	•
5 wt%	•	•	•
8.73 wt%		•	
15 wt%		•	•
20 wt%		•	
30 wt%		•	

For this study, Multimode V atomic force microscope from Bruker (Santa Barbara, USA) was used. High-sensitivity silicon cantilevers RTESPA (Bruker) were used for imaging in tapping mode AFM [41, 42]. These cantilevers have a nominal resonant frequency of 300 kHz and a nominal force constant of 40 N/m. The probe material is antimony (n) doped silicon with the nominal cantilever dimensions 125 × 35 × 3.5 μm^3. The cantilever has a chemically etched rotated silicon tip on its edge and the tip height is in the range of 15–20 μm with nominal tip radius of 8 nm.

The specimens were measured using tapping mode in air at +25 °C. In this dynamic mode the cantilever (AFM probe) is oscillated close to its resonance frequency while it is raster scanned across the sample surface. In this manner, the tip maintains in intermittent contact with the sample surface while keeping both the tapping forces (leading to undesired deformation or change of the sample) as well as the lateral forces at a minimum level. As the tip approaches the sample surface, the resonance frequency of the cantilever is altered due to the forces acting between the sample and the cantilever tip: so-called tip-sample interaction forces. As a consequence, amplitude and phase angle of the oscillating cantilever will change. The amplitude is maintained at a constant level by a feedback loop. The feedback parameters can be separated into surface topology information, and tip-sample interaction information. The latter, leading to the AFM phase images, provides the mechanical properties of the material probed.

Change in local surface topography or local material properties of the sample will be reflected in the tip-sample interaction force, and can lead to hysteresis between the approach and retraction of the cantilever in a tapping cycle. This hysteresis results from dissipative interaction between sample and tip. Thus, two principal datasets are the output of an AFM-experiment: topography and phase-lag, obtained simultaneously. Topography data provide information of relative height of the various features or the surface roughness as the probe tip is raster scanned across the

sample surface. The phase data channel in AFM measurements represents the phase lag of the cantilever response with respect to the driving signal. The acquired data build up a map of the surface topography which is presented as topography image. The phase lag provides a map of local phase. This, a phase contrast, provides the qualitative differences in local material properties of the measured sample.

The probe scan rate was chosen to 1.0 Hz (1 line/s) and overview scans of the microstructure were recorded at $30 \times 30\ \mu m^2$ scan size with a pixel resolution of 512×512. Details of the microstructure were obtained at scan sizes of $10 \times 10\ \mu m^2$ and a high resolution image for the original bitumen at $2 \times 2\ \mu m^2$ with the same scan rates and pixel resolutions as mentioned. The Gwyddion software package was used as an offline AFM image analysis tool [43].

4 Results and discussion

4.1 LVE behavior from CR testing

The creep response of the original and artificially produced bitumen samples, obtained from CR tests (described in Sect. 3.3), are presented in Fig. 3. Both diagrams show the evolution of the experimentally obtained creep compliance J over time. The left diagram presents the results in lin–lin scale, while the creep compliance is shown in logarithmic scale in the right diagram. CR tests were carried out with triple replication for all samples; the diagrams show the actual test data at +5 °C. Results from 0, 5, 20 and 30 wt% samples are from artificial bitumen, the results from the 8.73 wt% represent the original bitumen.

Three different phenomena can be identified from these results: (a) increasing asphaltene content leads to decreasing creep compliance implying stiffer material behavior, (b) the creep rate dJ/dt decreases with increasing asphaltene content until almost elastic behavior can be observed for an asphaltene content of 30 wt%, and (c) adding only low amounts of asphaltenes (5 wt%) to the maltene phase (labelled as 0 wt% asphaltenes in Fig. 3) causes an abrupt increase in stiffness. The creep compliance J comes to mean value (MV) of 87 MPa^{-1} for the 0 wt% samples and to 17 MPa^{-1} for the 5 wt% samples after 1,800 s. Thus, the stiffness increases by the factor of 5.1, indicating a structure in bitumen introduced by adding asphaltenes, which strongly influences the mechanical behavior. In addition, it can be observed that results from the original bitumen sample (8.73 wt%) are in between data from the 5 and 20 wt% artificial bitumen samples. This clearly indicates that the artificial bitumen samples exhibit a valid LVE behavior. Further analysis, especially on multi-scale modeling on these data is presented in [35].

4.2 Microstructure from AFM

For the microstructural investigation using AFM, four bitumen samples are available, the original bitumen, its maltene fraction, the maltene doped with 8.73 and 30 wt% asphaltene. The microstructural morphology of these four bitumen samples, both in topography and phase images have been presented in Figs. 4, 5, 6 and 7.

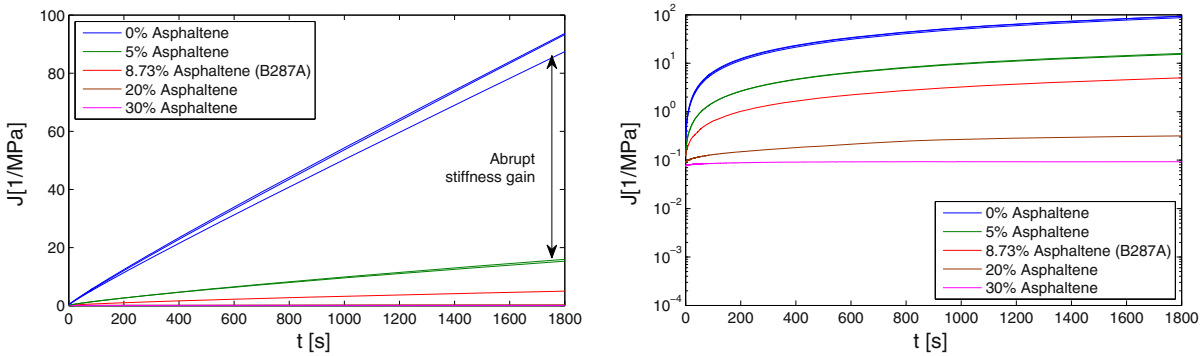

Fig. 3 Creep response of bitumen samples from CR tests at +5 °C

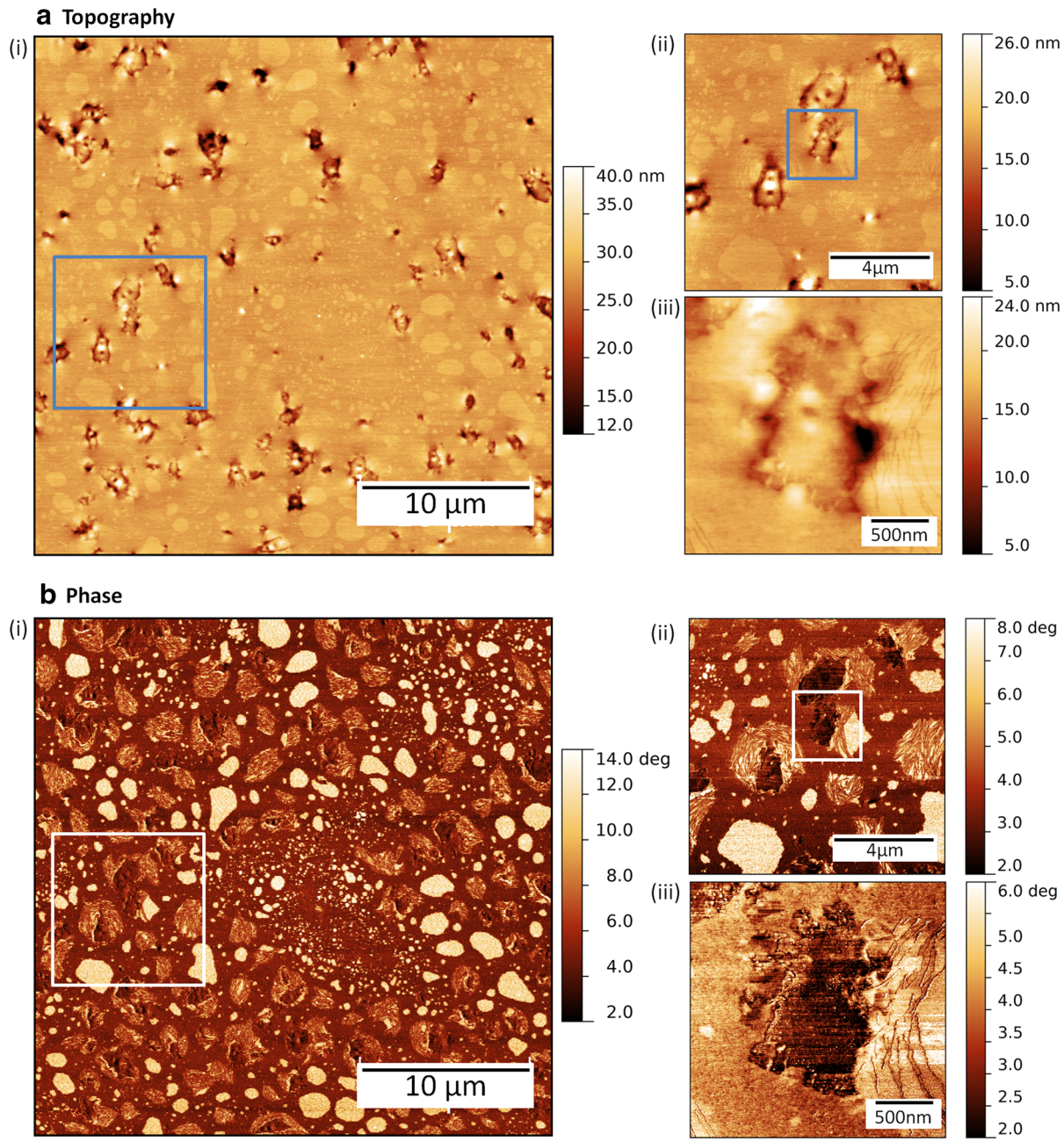

Fig. 4 Microstructure of original bitumen B287A: **a** AFM topography images, **b** AFM phase images of (*i*) 30 × 30 µm^2, (*ii*) 10 × 10 µm^2 and (*iii*) 2 × 2 µm^2

4.3 Microstructure of the original bitumen B287A

Microstructure morphology of the original bitumen B287A is presented as topography (Fig. 4a) and phase (Fig. 4b) images. Both images are accessible as a microstructural overview by 30 × 30 µm^2 images which exhibits the characteristic properties of the material [Fig. 4a(i) and b(i)]. With a resolution of 10 × 10 µm^2, microstructural details are shown in Fig. 4a(ii) and b(ii). A zoomed in domain phase is displayed by 2 × 2 µm^2 scans in Fig. 4a(iii) and b(iii) revealing the topography and phase images of a single domain respectively.

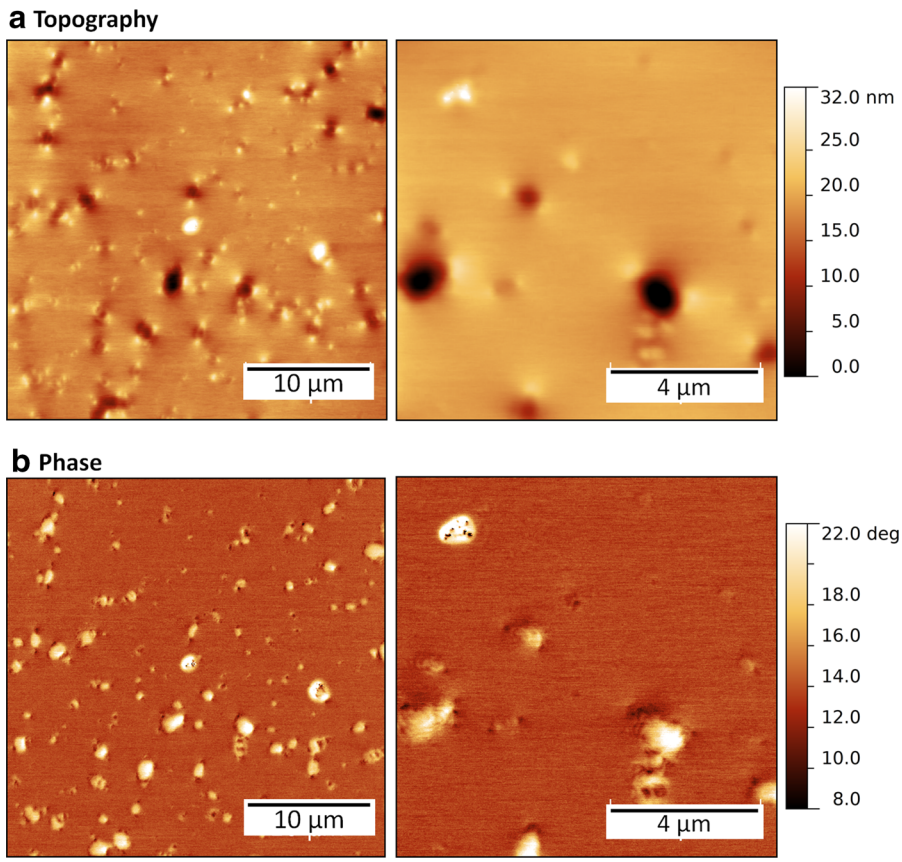

Fig. 5 Microstructure of the maltene fraction of original bitumen B287A: **a** AFM topography and **b** AFM phase images of both 30 × 30 and 10 × 10 μm^2

Four micro-phases are evident from the bitumen microstructure. A typical domain phase with a wrinkling along the long axis, most often termed as bee structure or catana phase, is observed to be dispersed over a continuous matrix phase (perpetua phase) [44–48]. The domain phase with wrinkling and the matrix phase are often considered to be the characteristic features of the bitumen microstructure [44, 47–50]. However, the precise morphology of the microstructure is known to be dependent on the bitumen origin and its thermal history [47].

Another phase, exhibiting a terraced pattern, is found adjacent to the domain phase where it partially encloses the domain phase [Fig. 4a(iii) and b(iii)]. This is rather distinct from many previous microstructural observations of bitumen; usually one finds that the terraced-crystallites completely surround the domains. Moreover, there are some independently occurring terraced structures over the matrix phase, which are not associated with the domain phase. Lastly, a new phase exhibiting a circular shape form appears on the matrix phase, which is not commonly observed in a bitumen microstructure.

From the phase images, it is noticeable that the average phase shift of the domain phase is comparable to the continuous phase, which indirectly suggests that the cumulative effect of the material property (stiffness, adhesion of the probe to the material) is identical in these two regions which is again a deviation from representative properties observed in common bituminous materials. Because, in most materials, this domain phase usually introduces higher phase shift than the continuous phase. However, for this particular bitumen the source of highest phase shift is found in the circular domains with a phase angle shift of 6 ± 0.8° to that of the domain phase whereas the other terraced-crystalline phase has a phase shift of 3 ± 0.5°.

From the topography images, again a correlation between domain size and appearance of the characteristic wrinkles can be found, as was observed in earlier studies [46]. The length along the long axis which is designated as the size of the domain phase varies from 0.25 to 2.60 µm in this bitumen. It is found that, for this bitumen, a minimum domain size of 0.85 ± 0.10 µm is required as a threshold for a characteristic wrinkling to appear in the

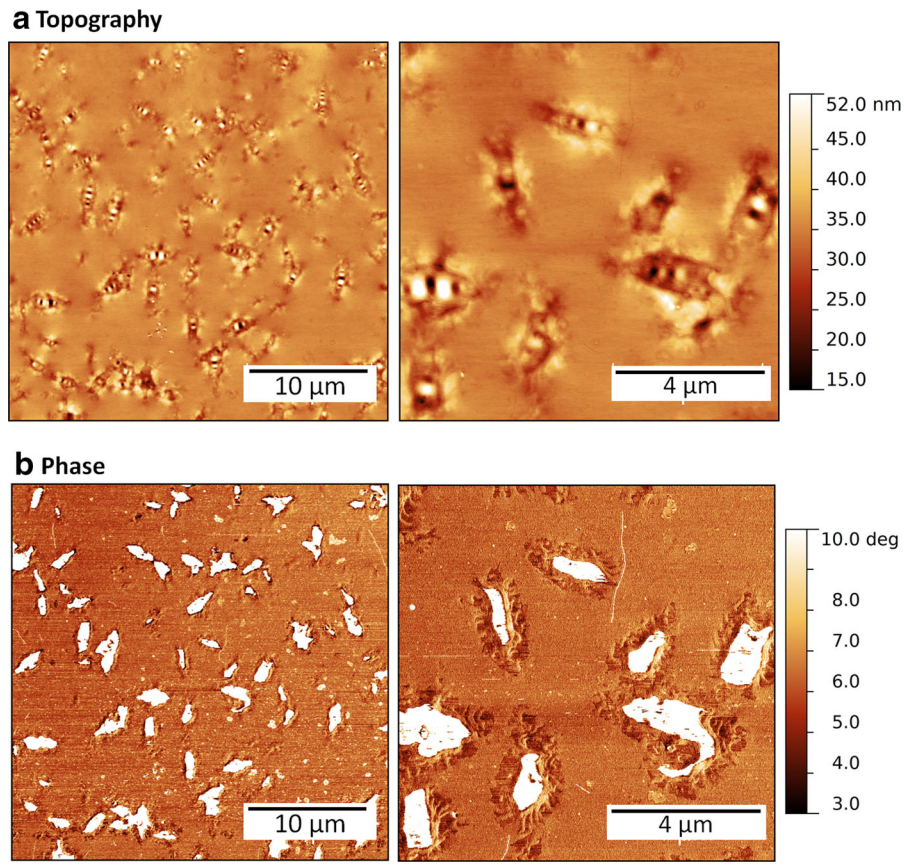

Fig. 6 Microstructure of 8.73 wt% asphaltene sample: **a** AFM topography and **b** AFM phase images of both 30 × 30 and 10 × 10 μm^2

domain phase. The circular phase of this bitumen possesses a bimodal size distribution with mean values of 0.32 ± 0.1 and 1.52 ± 0.32 µm at lower and higher range respectively and the contour of this phase is more clearly accessible from the phase images (Fig. 4b).

The various phases that emerge from AFM phase images represent areas with molecules that interact in a similar way with the AFM cantilever tip. In this sense these molecules can be considered chemically alike. New phases, like the "circular phase", are usually not observed in original bitumen.

4.3.1 Microstructure of the 0 wt% asphaltene sample (maltene phase)

The microstructure of the maltene phase of original bitumen B287A is presented in Fig. 5 as a topography (Fig. 5a) and phase (Fig. 5b) image wherein each consists of an overview image of 30 × 30 μm^2 and a high resolution 10 × 10 μm^2 scan size.

Unlike the original bitumen, only two major phases are observed in this fraction of the bitumen. An appearance of globular features other than an established domain phase is found to be dispersed over a continuous matrix phase. One of the key observations from the images is that the characteristic wrinkling does not appear in the topography. Moreover, the terraced-crystallites and the circular features are also absent in the morphology.

From the topography images in Fig. 5a it is evident that the globules often appear as random cavities or protrusions from the surface. The size of the globules varies from 0.20 to 1.60 µm. The exact contour or the interface of this phase to the matrix phase is easily obtained from the phase images in Fig. 5b.

4.3.2 Microstructure of the 8.73 and 30 wt% asphaltene artificial bitumen samples

Addition of 8.73 and 30 wt% asphaltene to the maltene fraction gives rise to different microstructure

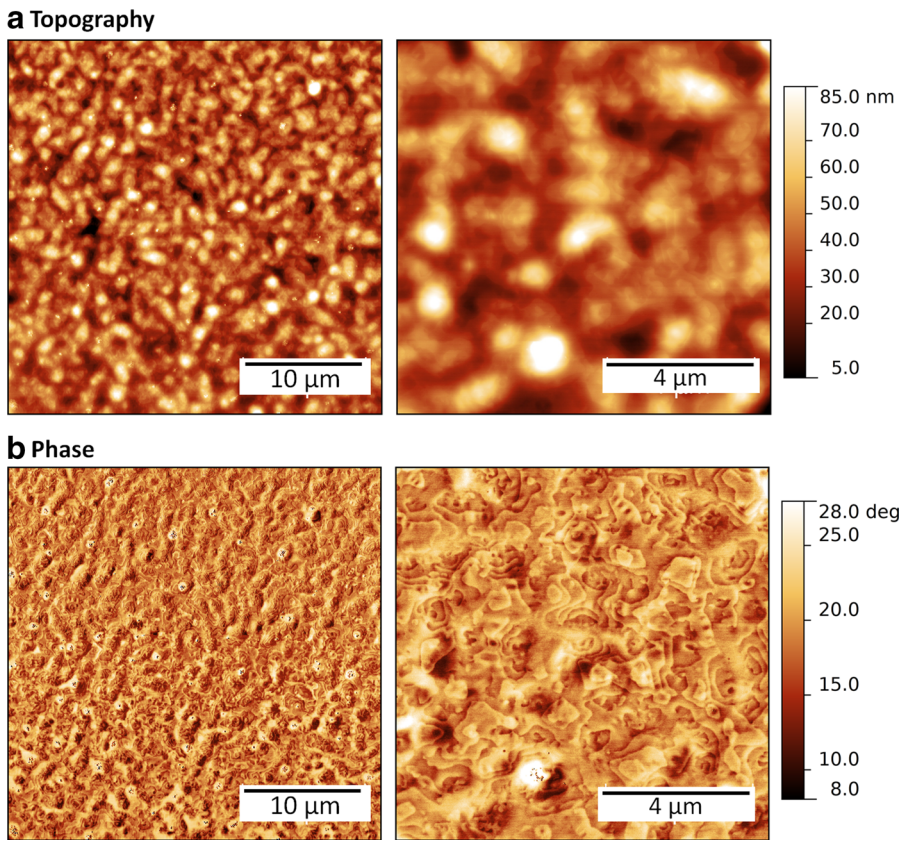

Fig. 7 Microstructure of 30 wt% asphaltene sample: **a** AFM topography and **b** AFM phase images of both 30 × 30 and 10 × 10 μm^2

morphologies. Firstly, the microstructure of maltene fraction doped with 8.73 wt% asphaltene is presented in Fig. 6, wherein topography images are shown in Fig. 6a and phase images in Fig. 6b. Further on, the microstructure of an artificial bitumen sample with 30 wt% of asphaltenes is presented in Fig. 7, wherein Fig. 7a and b are the topography and phase image respectively. Here, each topography and phase image consists of an overview image of 30 × 30 μm^2 and a high resolution 10 × 10 μm^2 scan sizes.

The morphology of 8.73 wt% asphaltene doped bitumen shows the evidence of restoration of characteristic microstructural features in the bitumen. The topography images in Fig. 6a display the domains of 1.20–3.90 μm with the wrinkled or the bee structure dispersed on a continuous matrix phase. The phase images reveal a 5 ± 0.5° phase shift between the bee structure and the matrix phase. The come-back of the typical bitumen morphology, displaying the domains with the bee structure dispersed over a matrix phase with the addition of asphaltenes, is a new observation.

At higher asphaltene dosage of 30 wt% to the maltene fraction, the microstructure of the bitumen changes drastically. The surface appeared to be entirely covered with agglomerated blobs and gave rise to a rougher morphology (z_{max} ~ 85 nm) in comparison to the other bitumen samples. Besides, the size of these blobs ranges from 0.80 to 2.20 μm. The characteristic features like domain or matrix phases of the original bitumen microstructure are absent in this bitumen. This may be explained as follows: asphaltenes are the more polar molecules in the molecular mix. At lower dosages, this leads to the formation of the characteristic bitumen microstructure. Increasing the asphaltene content eventually leads to a transition to a new phase pattern; this may be a similar effect as the transition associated with passing the percolation threshold. The high resolution phase image, 10 × 10 μm^2 scan in Fig. 7b displays the terraced pattern of the blobs with the average step size of 0.50 ± 0.15 μm. The steps of the terraced pattern are marked by profiles number 1 and 2 shown in the Fig. 8a. The step size for these two profiles is shown in Fig. 8b.

These two profiles are arbitrary examples but the average value with the standard deviation has been obtained from 30 profiles drawn in different locations on the high resolution AFM phase image (10×10 μm^2) of the sample.

A qualitative comparison of microstructural properties between the binder samples is presented in Table 3. The morphology resulting from the bitumen's maltene fraction doped with asphaltene fraction is found to have a strong dependence on the added amount of asphaltene. But the exact interaction, which may have contributed to the specific molecular association, is still not well understood and topic of ongoing research.

5 Summary and outlook

A better understanding of bitumen's composition, its microstructure and the impact of the microstructure on the mechanical behavior opens up possibilities to optimize the bitumen composition on the micro-level for e.g. better resistance to oxidative aging. Thus, durability of asphalt mixes can be enhanced as well. Expanding the multi-scale model for asphalt mixes by taking bitumen's microstructure into consideration is one way to analyze the impact of bitumen's microstructure on its LVE behavior. To implement the microstructure into the multi-scale model, the mechanical behavior of each constituent (maltene phase and asphaltenes) has to be obtained.

Thus, the presented study analyzes whether artificial bitumen samples with pre-defined asphaltene concentrations artificially made from *n*-heptane separated maltene and asphaltene phase are valid bitumen-like materials in terms of mechanical behavior and microstructure. In addition, the impact of asphaltene concentration in the samples is studied as well.

An unmodified bitumen 70/100 pen was separated into the *n*-heptane soluble (maltene) and insoluble (asphaltene) phase. Artificial bitumen samples with asphaltene concentrations from 0 to 30 wt% were produced from the two phases. The artificial bitumen samples as well as the original bitumen (8.73 wt% asphaltenes) were tested on their LVE behavior in the dynamic shear rheometer (DSR) by CR tests between -15 and $+5$ °C. The same samples were also analyzed by AFM on their microstructure. The results can be summarized as follows:

- Asphaltenes play an important role for the LVE behavior of the samples. Adding only low amounts of asphaltenes (5 wt%) to the pure maltene phase results in 5.1 times higher stiffness, indicating a network structure being introduced with adding asphaltenes.
- The creep rate dJ/dt decreases with increasing asphaltene concentrations, indicating asphaltenes to be responsible for the elastic part of bitumen behavior.
- A comparison between the original bitumen and the artificial bitumen samples show that they react similar in terms of LVE behavior, indicating that the artificially produced samples are valid for further mechanical analysis and as input data for multi-scale modeling.
- Microstructural analysis using AFM of the pure maltene phase exhibits two major phases—globular features dispersed over a continuous matrix. Wrinkling (bee structures), which is a typical feature for bitumen microstructure, does not appear in the maltene phase. This can be seen as a sign that the occurrence of wrinkling structures is connected with asphaltenes.
- The artificial bitumen sample with 8.73 wt% asphaltenes (equal to the original bitumen) shows clear evidence of restoration of characteristic microstructural features known from bituminous binders. The bee structure within the continuous matrix is restored in the artificial bitumen, showing that the addition of asphaltenes lead to a microstructure similar to natural bitumen. Thus, it can also be stated from the microstructural point of view that artificial bitumen samples precipitated from maltenes and asphaltenes are valid bitumen-like materials.
- High asphaltene concentration (30 wt%) leads to a drastic change in microstructure: agglomerated blobs with a rough morphology occur, no domain or matrix phase can be visualized. Here it is speculated that the observed radical change of morphology, may originate from a percolation-like transition which appears to be associated with the asphaltene concentration.

Based on the results of this paper, the extension of the multi-scale model for asphalt mixes allowing for the mechanical description of the LVE bitumen behavior depending on its composition is presented [35] and [36]. Within these papers, a structural RVE

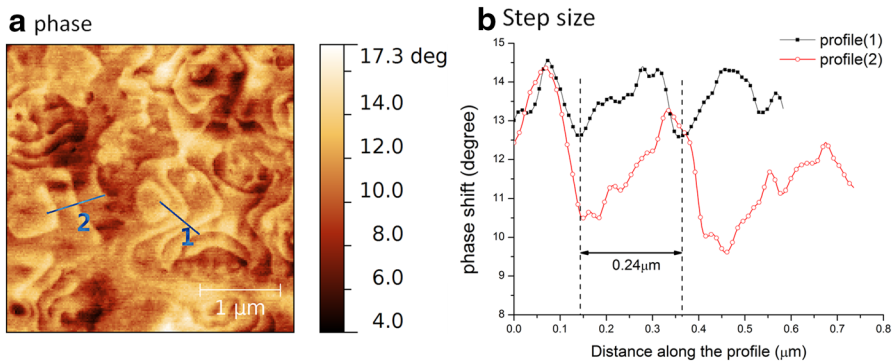

Fig. 8 **a** Cropped data from the 10 × 10 µm^2 AFM phase image of 30 wt% asphaltene sample exhibiting the terraced pattern and the steps are marked by 1 and 2 and **b** distance along the steps

Table 3 Microstructural characteristics of original bitumen, maltene fraction, maltene doped with 8.73 and 30 wt% asphaltene

Microstructural characteristics	Original bitumen	0 wt% asphaltenes (pure maltenes)	8.73 wt% asphaltenes	30 wt% asphaltenes
No. phases observed	4	2	3	1
Dominant phase	Domains (partially) surrounded by terraced structure	Matrix	Domains surrounded by terraced structure	Agglomerated blobs
Appearance of domain phase	Isolated domains	–	Isolated domains with occasional clusters	–
Wrinkling (domains)	Present	Absent	Present	Absent
Size range of surface structures	Domains 0.25–2.60 µm	Globules 0.20–1.60 µm	Domains 1.20–3.90 µm	Blobs of terraced structures 0.80–2.20 µm

concept based on SARA fractions is suggested, which is not only able to reproduce experimental results but also to describe significant microstructural effects related to aging.

Further questions have been raised by the study presented in this paper. Next steps within the research groups are to investigate why the pure maltene phase still shows a two-phase structure. *N*-heptane separation removed all asphaltenes (*n*–heptane insoluble by definition), but a certain share of micelles might be left from highly polar resins. A further separation of bitumen by *n*-pentane or *n*–hexane would result in different maltene phases with different microstructure and mechanical behaviour [5, 51]. Also, the procedure presented exemplarily within this paper for one bitumen will be run on more bitumen samples to verify the findings, as well as include polymer-modified binders.

Acknowledgments The authors would like to thank the Austrian Research Promotion Agency (FFG) for funding part of the presented research within the research project "Oekophalt", as well as to Mr. Thomas Riedmayer for running the mechanical bitumen tests for this study.

References

1. OECD (2013) Spending on infrastructure 1995–2011—trends, policies, data. International Transport Forum of the OECD, Paris, p 58
2. CEN (2012) EN 12597: Bitumen und Bitumenhaltige Bindemittel—Terminologie. CEN, Brussels, p 18
3. Merino-Garcia D et al (2010) Petrophase 2009 panel discussion on standardization of petroleum fractions. Energy Fuels 24(4):2175–2177
4. ASTM (2001) ASTM D 4124-01: standard test methods for separation of asphalt into four fractions. ASTM, Philadelphia, p 6
5. Lesueur D (2009) The colloidal structure of bitumen: consequences on the rheology and on the mechanisms of bitumen modification. Adv Colloid Interface Sci 145(1–2):42–82
6. Corbett LW (1969) Composition of asphalt based on generic fractionation, using solvent deasphaltening, elution-adsorption chromatography, and densimetric characterization. Anal Chem 41:3

7. Read J, Whiteoak D (2003) The shell bitumen handbook, 5th edn. Thomas Telford Ltd, London, p 464
8. Solaimany Nazar AR, Rahimi H (2009) Investiagtion on agglomeration-fragmentation processes in colloidal asphaltene suspensions. Energy Fuels 23(2):8
9. Sheu EY (1996) Physics of asphaltene micelles and microemulsions—theory and experiment. J Phys 1996(8):17
10. Fawcett A, McNally T (2003) Polystyrene and asphaltene micelles within blends with a bitumen of an SBS block copolymer and styrene and butadiene homopolymers. Colloid Polym Sci 281(3):203–213
11. Eyssautier J et al (2012) Organization of asphaltenes in a vacuum residue: a small-angle X-ray scattering (SAXS)–viscosity approach at high temperatures. Energy Fuels 26(5):2696–2704
12. Pollack SS, Yen TF (1970) Structural studies of asphaltics by X-ray small angle scattering. Anal Chem 42(6):7
13. Tripadus V et al (2004) The study of diffusive motion in bitumen compounds by quasielastic neutron scattering. Phys B 350(1–3):E455–E458
14. Yarranton HW et al (2013) On the size distribution of self-associated asphaltenes. Energy Fuels 27(9):24
15. Haji-Akbari N et al (2013) A unified model for aggregation of asphaltenes. Energy Fuels 27(5):2497–2505
16. Durand E et al (2010) Effect of chemical composition on asphaltenes aggregation. Energy Fuels 24(2):1051–1062
17. Mikula RJ, Munoz VA (2000) Characterization of emulsions and suspensions in the petroleum industry using cryo-SEM and CLSM. Colloids Surf A 174:14
18. Bearsley S, Forbes A, Haverkamp RG (2004) Direct observation of the apshaltene structure in paving-grade bitumen using confocal laser-scanning microscopy. J Microsc 215(2):7
19. Forbes A et al (2001) Studies of the microstructure of polymer-modified bitumen emulsion using confocal laser scanning microscopy. J Microsc 204(3):252–257
20. Handle F, Füssl J, Neudl S, Großegger D, Eberhardsteiner L, Hofko B, Blab R, Grothe H (2014) The bitumen microstructure: a fluorescent approach. Mater Struct. doi:10.1617/s11527-014-0484-3
21. Seifried CM, Crawshaw J, Boek ES (2013) Kinetics of asphaltene aggregation in crude oil studied by confocal laser-scanning microscopy. Energy Fuels 27(4):1865–1872
22. Soenen H et al (2013) Laboratory investigation of bitumen based on round robin DSC and AFM tests. Mater Struct 47(7):16
23. Yu X et al (2013) A systematic AFM-based method to measure adhesion differences between micron-sized domains in asphalt binders. Fuel 113:443–447
24. Champion-Lapalu L et al (2002) Cryo-scanning electron microscopy: a new tool for interpretation of fracture studies in bitumen/polymer blends. Energy Fuels 16(1):143–147
25. Loeber L et al (1996) New direct observations of asphalts and asphalt binders by scanning electron microscopy and atomic force microscopy. J Microsc 182(1):7
26. Lyne ÅL et al (2013) Surface wrinkling: the phenomenon causing bees in bitumen. J Mater Sci 48(20):6970–6976
27. Lu X et al (2005) Wax morphology in bitumen. J Mater Sci 40:8
28. Redelius P (2011) Asphaltenes in bitumen, what they are and what they are not. Road Mater Pavement Des 10(1):18
29. Sourty ED et al (2011) The microstructure of petroleum vacuum residue films for bituminous concrete: a microscopy approach. J Microsc 241(2):132–146
30. Lackner R et al (2004) Multiscale modeling as the basis for reliable predictions of the behavior of multi-composed materials. Prog Eng Comput Technol 8:153–187
31. Lackner R et al (2005) Is low-temperature creep of asphalt mastic independent of filler shape and mineralogy? Arguments from multiscale analysis. J Mater Civ Eng 17(5):485–491
32. Aigner E, Lackner R, Pichler C (2009) Multiscale prediction of viscoelastic properties of asphalt concrete. J Mater Civ Eng 21:771–780
33. Pichler C, Lackner R (2009) Upscaling of viscoelastic properties of highly-filled composites: investigation of matrix-inclusion type morphologies with power-law viscoelastic material response. Compos Sci Technol 69:2410–2420
34. Pichler C, Lackner R, Aigner E (2012) Generalized self-consistent scheme for upscaling of viscoelastic properties of highly-filled matrix-inclusion composites—application in the context of multiscale modeling of bituminous mixtures. Compos B 43:457–464
35. Eberhardsteine L, Füssl J, Hofko B, Handle F, Hospodka M, Blab R, Grothe H (2014) Influence of asphaltene content on mechanical bitumen behavior: experimental investigation and micromechanical modeling. Mater Struct 1–14. doi:10.1617/s11527-014-0383-7
36. Eberhardsteiner L, Füssl J, Hofko B, Handle F, Hospodka M, Blab R, Grothe H (2015) Towards a microstructural model of bitumen aging behavior. Int J Pavement Eng. doi:10.1080/10298436.2014.993192
37. CEN (2007) EN 1426: bitumen and bituminous binders—determination of needle penetration. CEN, Brussels
38. CEN (2007) EN 1427: bitumen and bituminous binders—determination of the softening point—ring and ball method. CEN, Brussels
39. CEN (2005) EN 14770: bitumen and bituminous binders—determination of complex shear modulus and phase angle—dynamic shear rheometer (DSR). CEN, Brussels
40. CEN (2005) EN 14771: bitumen and bituminous binders—determination of the flexural creep stiffness—bending beam rheometer (BBR). CEN, Brussels
41. Eaton PW (2010) Atomic force microscopy. Oxford University Press, Oxford
42. Garciá R, Pérez R (2002) Dynamic atomic force microscopy methods. Surf Sci Rep 47(6–8):197–301
43. Nečas D, Klapetek P (2011) Gwyddion: an open-source software for SPM data analysis. Cent Eur J Phys 10(1):181–188
44. Masson JF, Leblond V, Margeson J (2006) Bitumen morphologies by phase-detection atomic force microscopy. J Microsc 221(1):17–29
45. Nahar S et al (2013) First observation of blending-zone morphology at interface of reclaimed asphalt binder and virgin bitumen. Transp Res Rec 2370(1):1–9
46. Nahar SN et al. (2014) Turning back time: rheological and microstructural assessment of rejuvenated bitumen. TRB 93rd annual meeting compendium of papers, 1–17
47. Nahar SN et al (2013) Temperature and thermal history dependence of the microstructure in bituminous materials. Eur Polym J 49(8):1964–1974
48. Schmets A et al (2010) On the existence of wax-induced phase separation in bitumen. Int J Pavement Eng 11(6):555–563
49. Pauli AT et al (2001) Atomic force microscopy investigation of SHRP asphalts. Abstr Pap Am Chem Soc 221:U220

50. Stangl K, Jäger A, Lackner R (2006) Microstructure-based identification of bitumen performance. Road Mater Pavement Des 7(sup1):111–142

51. Merino-Garcia D et al (2010) Petrophase 2009 panel discussion on standardization of petroleum fractions. Energy Fuels 24(4):2175–2177